Chapter 4: The Forward Muon System.

Introduction

The H1 Forward Muon Spectrometer is designed to identify and measure the momentum of muons in the forward direction ($4° < \theta < 17°$). The system consists of six double planes of drift chambers and an iron toroid, as illustrated in figure 4.1. The detector hardware hierarchy is shown in figure 4.2.

The active detector area is split into two sections, before the toroid and after the toroid (before and after here are for a particle originating from the H1 vertex, i.e. travelling in the same direction as the proton beam). Each of these sections consists of three double layers of drift chambers, two with wires strung around the beam pipe and one with wires strung radially out from the beam pipe. A layer is also radially segmented into octants, each octant being mounted on its own octant frame.

Figure 4.1: The forward muon spectrometer. From [30].

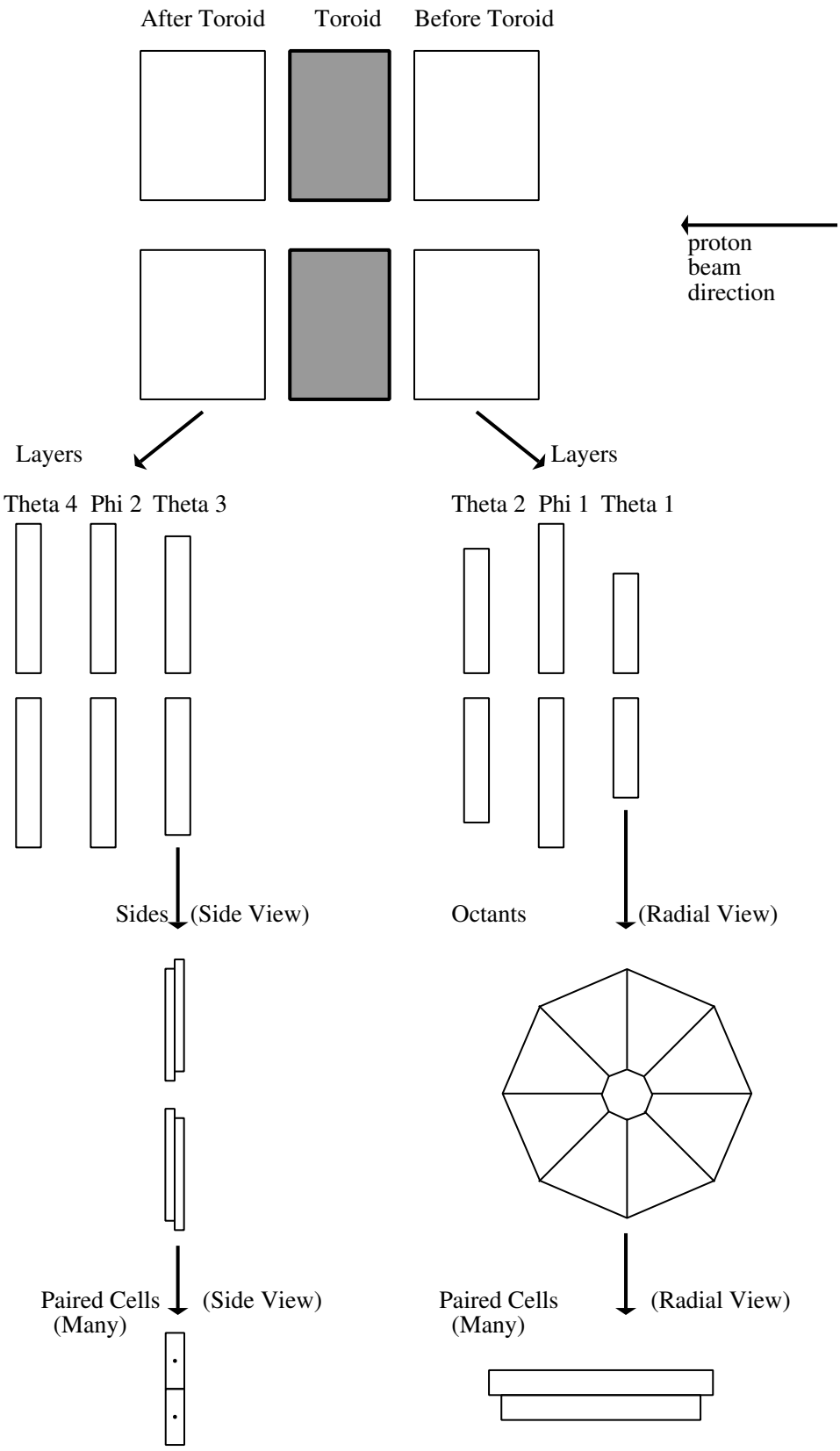

Figure 4.2: The forward muon system hardware hierarchy.

Within one side of an octant the cells are arranged into pairs, connected together using a 330 Ω resistor. This halves the amount of readout electronics required for the detector, at the expense of introducing more resistance into the system and hence creating greater pulse attenuation. The cells on each side of a layer are offset by half the width of a cell, allowing resolution of drift sign ambiguities and extraction of an independent T_{zero} by the forward muon trigger.

Principle Of Operation

The basic principles of operation of the forward muon system are show in figure 4.3. A charged particle passing through the system leaves a trail of ionised gas in the chambers through which it has passed, figure 4.3(a). An electric field is maintained in each cell so that the electrons produced by this ionisation drift toward the sense wire at the centre of the cell and the positive ions drift towards the cell walls. A potential difference is maintained between the sense wire and the drift voltage in the cell, such that when the ionisation electrons approach the wire they experience a strong radial field. This accelerates the electrons so that they can cause further ionisation in the gas near the wire, creating an avalanche of electrons and hence a larger signal, an effect known as gas amplification, figure 4.3(b).

These charges produce pulses on the sense wire which are then collected by the readout system. Analysis is done online to give information on the time taken for the first electrons to drift from the path of the particle to the wire and the integrated charge collected at the two wire ends, figures 4.3(c) to (k). This is referred to as Qt information.

In the offline reconstruction program, the Qt values are converted to space points, figures 4.3(l) and (m). As the drift time contains no information on which side of the sense wire the particle passed, there is an ambiguity in the sign of the drift co-ordinate. This ambiguity may be resolved by looking for a corresponding hit in the other side of the double layer. As the sides are offset by half a cell, two hits may line up to form a pair as shown in figure 4.3(n).

Once pairing has resolved the drift sign ambiguity, track segments before and after the toroid are formed by considering all possible combinations of pairs. The chi-squared (χ^2) method is used to assess quality of fits, as described later. The value of χ^2 for each straight line

fit is calculated and those pairs that satisfy a cut are accepted. The track segments before and after the toroid are then associated as possible track candidates, figures 4.3(o) and (p). A series of extrapolations is then carried out for each each track candidate assuming a range of momenta and a χ^2 calculated for each possibility, figures 4.3(q) to (u). The value of momentum giving a minimum for this χ^2 is then taken to be the momentum of the track (assuming that the minimum value of χ^2 is less than a cut). Reconstruction is now complete and other subdetector information may be linked to the forward muon information, but this linking will not be described further.

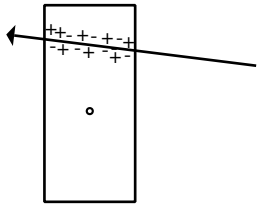

a) A charged particle passes through a cell producing a number of electron-ion pairs.

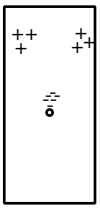

b) The electrons drift towards the wire, the ions drift (more slowly) towards the cell walls. Once the electrons get close to the wire, the strong radial field produces an avalanche.

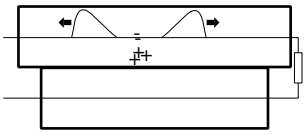

c) The avalanche produces a pulse in the wire which propagates in both directions along the sense wires of the two linked cells.

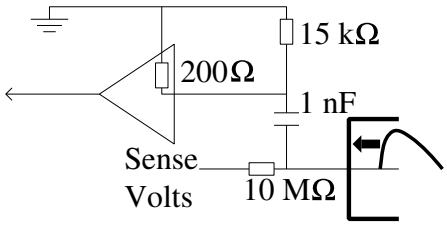

d) As the pulse propagates along the wire, the different frequencies travel at different velocities. The net result is that the leading edge steepens while the trailing edge becomes more spread out. The pulse reaches the pre-amplifiers at the end of the cells and is picked off the sense wire by a 1 nF capacitor.

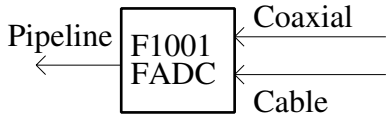

e) The preamplified pulses from both wire ends are fed through 50 m coaxial cables to an F1001 Flash Analogue to Digital Converter. Here, they are digitised into 9.6 ns bins and stored in a 256-bin pipeline.

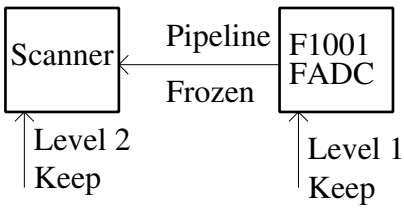

f) When a level one trigger keep signal is received, the FADC sampling is stopped, freezing the last 256 time bins in the pipeline. When a level two trigger keep signal is received, the scanner reads out the pipeline into its own buffer.

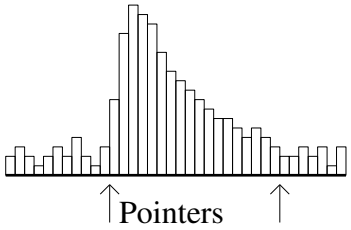

g) As the data are being read out, pulse height analysis is carried out upon the samples. Pointers are created to mark when the signal crosses a threshold value and remains above it for a number of bins. A second pointer is created for when it falls below threshold for a second number of bins.

Figure 4.3 (a-g): The stages of particle detection and reconstruction in the forward muon system. Stages d,e,f,g form the readout chain of the chambers.

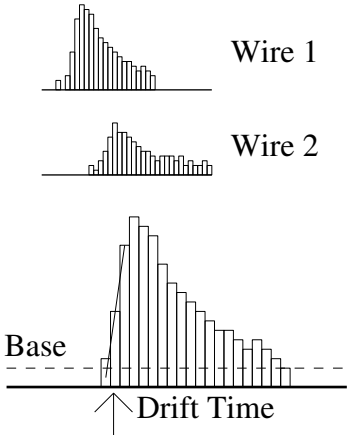

h) The signals from the two wire ends are compared. If pulses exist on both within a certain time of each other they are associated. If not, the pulse is retained but flagged as single-ended. This can occur when the hit is near the preamp of one wire end and thus the pulse on the other wire end is small.

i) Drift time extraction is performed. This is based on extrapolating the leading edge back to the background (or base) level, then taking the time to be a constant fraction along the leading edge from this time. An event T_{zero} is required from the central trigger to give the starting point for drift time.

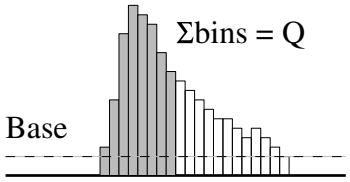

j) Charge integration is performed. The signal is summed for eight time bins unless either associated pulse is less than 8 bins long in which case this shorter pulse length is used. The signal is corrected to start at the obtained drift time instead of the first channel in the pulse. Finally, the pedestal is subtracted.

MRTE	Chan	Q(1)	Q(2)	···
Hit 1				
Hit 2				
Hit 3				
...				

k) The event is assembled by the event builder and the Qt information is stored in the MRTE BOS-bank (MRPE for phi chambers). This is the end of the online processing and data aquisition chain.

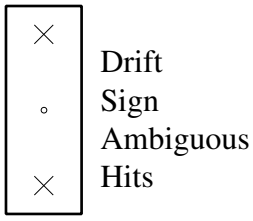

l) Offline, the drift time information is converted to a drift distance using the drift velocity and wire t_{zero} information. This gives a distance but not a direction, so the information has drift sign ambiguity. The drift distance errors are ≈250 μm.

m) The charges on the two wire ends are used in the charge division algorithm (Q(1)-Q(2))/(Q(1)+Q(2)) to determine how far along the wire the hit occurred. Single ended hits are placed at the preamp end of the wire that gave the signal. Charge division errors are ≈1% of wire length, that is, of order of centimetres.

n) Pair finding is carried out on both sides of a layer. Hits are required to be within a certain distance of each other in drift and charge division co-ordinates to be paired. No vertex pointing is required. Hits not associated into pairs are retained but are flagged as being unpaired hits.

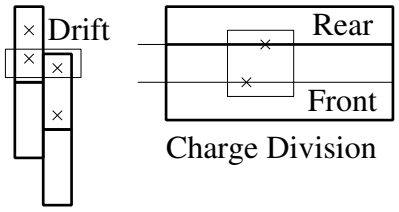

Figure 4.3 (h-n): The stages of particle detection and reconstruction in the forward muon system. h,i,j together form the Qt analysis which may be performed on the front end processor (as assumed here), on the level 4 filter farm or offline.

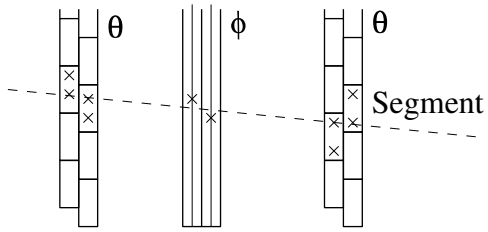

o) Track segments are formed from pairs. At least one pair is required in a theta layer, plus at least an unpaired hit in the other theta layer. Nearby hits in the phi chambers are associated with the segment.

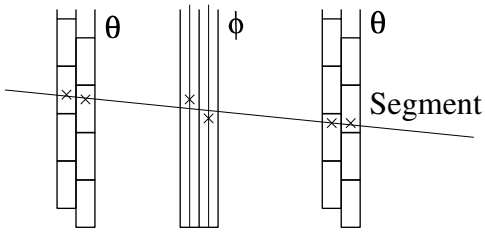

p) The track segments are assessed on the basis of a χ^2 fit. Drift ambiguities are resolved at this stage. A single pair may be used in more than one segment, but no two segments may differ only in the drift sign ambiguity resolution of the component hits: the one with the lowest χ^2 is taken.

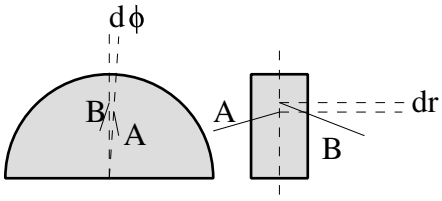

q) Track segments before and after the toroid are compared. For each segment after the toroid, a search is made for segments before the toroid that lie within a certain distance in the radial and phi co-ordinates, dr and dϕ, defined at the central plane of the toroid.

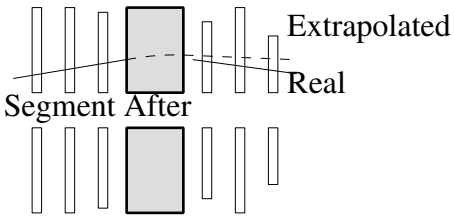

r) For each track candidate, a momentum determination is made by extrapolating from the segment after the toroid for several values of momentum. A χ^2 is calculated based on the difference between the extrapolated segment and the actual segment.

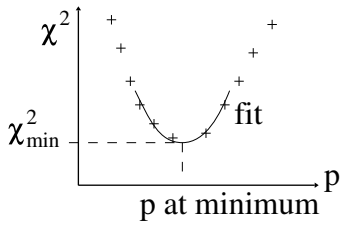

s) The minimum value of the χ^2 for the track candidate is calculated by fitting a quadratic to the points around the lowest value found in the scan. If this minimum value exceeds a cut, the candidate is rejected. The track is assigned the momentum corresponding to this minimum value.

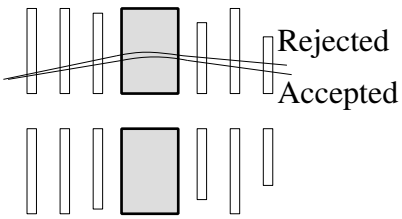

t) All tracks are compared to ensure that no hit has been used more than once. Segments may be formed with both signs of drift ambiguity, and these duplicates are now rejected so that only the candidate with the lowest track χ^2 remains.

MTKR	1/p	Theta	Phi	···
Track1				
Track2				
Track3				
...				

u) The final track information is stored in the MTKR BOS bank and written to the output stream. Forward muon reconstruction is now complete. Other software modules may now attempt to link the MTKR tracks with tracks elsewhere in the detector.

Figure 4.3 (o-u): The stages of particle detection and reconstruction on the forward muon system.

The Drift Cells

Figure 4.4 shows a cross section through four forward muon drift cells mounted on an aluminium octant frame. The cells are built from two planes of printed circuit board (PCB). These boards are coated on both sides with copper: the outer surface is kept at ground to screen the cell whereas the inner board has been machined to form 19 copper strips, 4mm wide with 2mm gaps except for the first and last strips which are thinner to partially compensate for edge effects. These two layers of PCB are held 2.0 cm apart by 0.7mm thick aluminium extruded side profiles, again held at ground. The strips on the interior of the cell are connected via 230 MΩ metal film resistor chain to the drift high voltage power supply to produce the drift field in the cell. The nominal drift voltage is 3 kV, producing an average drift field of 0.45 kV cm^{-1}.

Along the long axis of each cell runs a Nichrome sense wire, 20 μm in radius for the short inner cells and 25 μm for the longer outer cells. Wires more than 1.5 m long have a support at the mid-point of the cell. The wire is kept at positive high voltage, notionally 4.5 kV, which ensures a potential difference of 1.5 kV between the centre of the drift field and the wire. This potential difference produces a radial field around the wire which is responsible for the gas amplification of the primary pulses.

The cell endcaps are made of moulded Noryl with a precise dowel hole for fixing the cell to the octant frame with a precision of 50 μm in the drift direction and 1 mm in the other directions. Both endcaps contain wire crimps to hold the sense wire and holes for the gas supply to the chambers. One endcap also contains the resistor chain, high voltage connectors for the drift voltage and sense voltage and the sense wire readout, which is decoupled from the DC sense voltage supply by a 1 nF ceramic disk capacitor. The other endcap contains a sense wire connection via a 330 Ω resistor to the sense wire of the adjacent cell.

The connection between two cells forms a readout pair. Ideally, both ends of each wire would be read out to obtain the charges at the two wire ends for charge division. However, connecting two cells together allows the detector to be read out using only half the number of channels.

Figure 4.4: Cross-section of forward muon drift cells mounted on an octant frame. From [50].

Greater pulse attenuation is introduced when using pairs linked by a resistor as the pulse has to travel through a greater length of wire. This can be a problem when the hit is close to one of the preamplifiers as the pulse on the far wire end may be so attenuated that it cannot be resolved from the pedestal. Such hits, with a large pulse on one wire end and no pulse on the other wire end, are called single-ended hits.

The Gas System

The chamber gas is supplied from a recirculator in the main H1 gas room. The gas mix used in Autumn 1992 was 92.5% Argon, 5.0% Carbon Dioxide and 2.5% Methane. The composition of the mixture is optimised to satisfy several criteria. The signal produced in the chambers originally comes from ionisation produced by the passage of a charged particle so one requirement of the gas is that it should be easy to ionise, such as a noble gas. A quenching agent is added to prevent the gas from breaking down and discharging continuously.

The drift velocity of the gas is dependant primarily on the gas mixture, the applied electric field (E) and the pressure (p). The dependence on other parameters, such as temperature and applied magnetic field, is comparatively weak. Figure 4.5 shows the variation in drift voltage versus electric field over gas pressure. The region where the drift velocity only varies slowly with changes in E/p is called the plateau. It is advantageous to operate in this region because minor variations in E or p will not affect the drift velocity significantly.

The drift velocity of the gas must be chosen as a compromise between two conflicting requirements. First, the time resolution of the system is roughly constant as the shape of the pulses produced does not depend strongly on the drift velocity. This means that a long drift time and hence a low drift velocity is desirable to achieve high spatial precision. The second requirement is that the chamber signal must be delivered in a short enough time for the forward muon trigger to be able to produce a decision. The nominal drift velocity of the final gas mix is 4.5 cm/μs.

Figure 4.5: Graph of the drift velocity versus E/p for the final Ar:CO_2:CH_4 gas mixture. From [30].

Readout Electronics

On reaching the wire, the electrons produce a pulse which then travels down the wire in both directions. The pulses at the wire ends are picked off the sense wire by a 1 nF capacitor and are then preamplified. These preamplified pulses are then digitised by F1001 Flash Analogue-to-Digital converters. The F1001 FADCs are clocked at 104 MHz, ten times the HERA clock frequency, and have a resolution of eight bits with a non-linear response, giving an eight bit resolution for small pulses with a 10 bit dynamic range. The result of the digitisation is fed into a 256 time bin pipeline (actually a 256 byte memory used as a circular buffer) where it is stored until a level one trigger signal is received or 256 clock signals have arrived, in which case it falls off the end of the pipeline. Up to 16 FADCs are present in each crate, plus a scanner unit and a front-end processor (described below) and other control cards which will not be discussed further.

Once a level one trigger keep signal is received, the sampling is frozen. If a level two trigger keep is received, the pipeline is read out by an M1070 scanner which analyses the pulses for hits crossing threshold and performs zero suppression on the signal. If a level two reject is received, the pipeline is unfrozen and sampling begins again.

When a level three trigger keep is received, the scanner sends an interrupt to the FIC 8231 front end processor in the crate. This processor now reads the hit pointer information created by the scanner and assembles the raw data into offline format raw data banks, called MRTD (for the theta chambers) and MRPD (for the phi chambers) banks. These banks contain the pulses identified by the scanner plus several (currently six) time-bins before the pulse start to allow dynamic pedestal subtraction. An intelligent decision is also made for the case when two hits occur close together on the same wire; if the tail of the first pulse might influence the second pulse, all bins are kept.

Hardware Organisation

The theta layers are constructed by mounting cells onto aluminium octant frames. All octant frames are identical, but not all cell positions are populated in a given layer. An octant of theta layer one has 12 cells on each side, starting at the lowest cell position. Theta two octants have 14 cells per side starting from the lowest position. Theta three octants have 18 cells per side but the lowest position is not filled. Theta four octants have 20 cells per side and again the lowest position is not filled. This gives a total of 1024 theta cells. The top right corner of the octant frames are truncated or 'cutoff' to allow the frames to fit into the H1 experiment hall.

All of the octants in a given theta layer are identical. However, in order to fit the frames into the H1 hall, alternate frames must be 'flipped' so that the cutoff corners lie at top, bottom, left and right, as shown in figure 4.6. In order to allow the chambers to fit together without gaps, a small overlap is provided at octant boundaries and so each octant is offset from its neighbour in z. Hence, the arrangement is two Maltese crosses, shown in figure 4.6, where the octants mounted in nearest H1 are marked '+', those further from H1 with '-'. The octants are mounted on each side of aluminium door frames with each door frame holding 2 octants and forming a quadrant. The four door frames are mounted on an iron layer frame. The door frames may be retracted to allow access to the beam line.

It was envisaged that the environment near the beam line might prove too hostile for the chambers to be operated safely. Hence, the inner six cells on each octant side have their own voltage control, independent of the outer cells, so that they may be turned off if necessary. As the phi chambers are radial, the long cells that extend to near the beam pipe are mounted on a movable frame called a slider. This arrangement is shown in figure 4.7 where the cells mounted on the slider are shaded grey. The sliders are mounted on the front of the octant frame, giving three 'sides' to a phi octant.

Phi layer 1 has 27 cells mounted on each octant, with the two left-most and two right-most positions on each side of the octant not filled. Phi layer 2 has 35 cells mounted on each octant. The odd number of cells per octant leaves one cell that has to be read out at both ends. This is referred to as an unlinked cell. This gives a total of 496 phi cells but 512 readout

channels, and 1520 cells in the whole system.

Figure 4.6: Theta layer four, showing cutoff orientation. Octants marked '+' are nearer H1, those marked '-' are further from H1.

Figure 4.7: A single phi octant. Shaded cells are on the slider. From [50].

The Toroid

The toroid is composed of two movable halves, each of which is composed of four semi-circular sections. The assembled halves are held together by iron bolts. The toroid may be opened to allow access to the beam line. The current is supplied by twelve rectangular coils, each of which is composed of fifteen turns of copper tubing, 11.5 mm square, with an 8.5 mm square hole through which cooling water flows. The assembled toroid is 1.2 m thick, with an inner radius of 0.65 m and an outer radius of 2.90 m. The nominal current in the coils is −150 Amps. The toroid is held together by six bolts.

The field is monitored by observing the change in flux as the magnet is switched on and off in 9 wire coils threaded through holes in the iron, producing a radial map of the field. There is a distortion where one of the coils includes a bolt as the bolt does not make good magnetic contact with the rest of the toroid. This is thought to distort the field in the adjacent coils as well. Figure 4.8 shows the position of the monitoring coils in the toroid.

The parameterisation used for the toroid magnetic field is

$$B_\phi = \frac{B_0}{r^{0.0932}}$$

where B_ϕ is the ϕ-component of the magnetic field in Tesla, r is the radial distance from the beam axis and B_0 is a current dependent constant. The radial and z-components of the field are assumed to be zero, and the field outside the toroid is also assumed to be zero. B_0 is related to the current in the coils, I, in Amperes, by the parameterisation

$$B_0 = \sum_{j=1}^{6} c_j \left(\frac{|I|}{100 \text{ Amps}} \right)^{j\text{-}1}$$

where the constants c_i are given by (from [52]):

$c_1 = +0.95918$ T $\quad c_2 = +0.13198$ T $\quad c_3 = -0.11112$ T

$c_4 = +0.52165$ T $\quad c_5 = -0.12564$ T $\quad c_6 = +0.12219$ T

The above parameterisation applies for a negative current in the toroid, and the field

produced is such that positively charged muons are de-focussed by the field. For positive currents, the value of B_0 is negated so positive muons are focussed by the field. Figure 4.9(a) shows the parameterisation of B_0. Figure 4.9(b) shows the measured and parameterised field for various values of the current in the coil. The penultimate point (at approximately 2.5 metres) is the coil containing one of the six bolts and this point and the points on either side are not used in the parameter fitting. It may clearly be seen from the figure that the parameterisation is not valid for $|I|<100$ Amps. The nominal operating current is -150 Amps and it is not foreseen to take physics data with a reduced current except for alignment data taken with zero magnetic field.

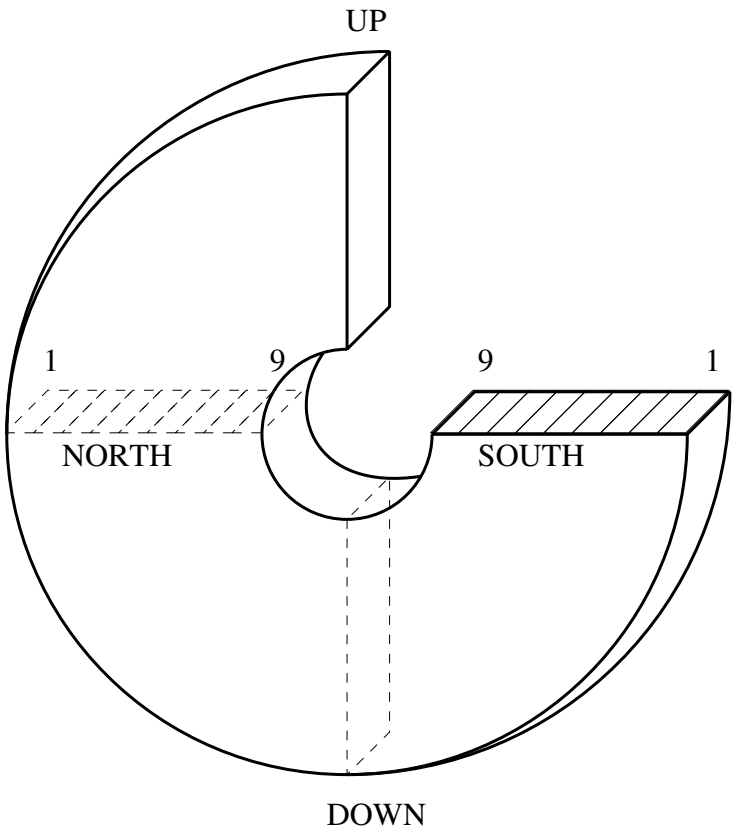

Figure 4.8: The forward muon toroid showing the position of the monitoring coils. The field strengths are measured in two sets (North and South) each of nine coils. There are also two large coils (Up and Down).

Figure 4.9: Parameterisation of the magnetic field in the toroid. a) B_0, b) field strength. From [52].

Qt Analysis

The purpose of the Qt analysis is to extract the drift time, t, (the time taken by the first electron in the ionisation droplet to drift from its original position to the wire) and the charge integrals for the leading edges of the two pulses, Q(1) and Q(2). This analysis may be performed by the front-end processor, by the level four filter farm or offline. A full description of the Qt algorithm may be found in [53].

The drift time determination uses a leading edge algorithm, as shown in figure 4.10. First, the background level LBASE is calculated by taking the average level of the pre-samples taken before the pulse. Then, for each pulse, the maximum difference in pulse height between successive samplings in the rising edge is identified. This difference is called MAXDOS. The centre of the second of the two samplings involved is labelled IMAXDOS, and a line of slope $MAXDOS^{-1}$ is drawn from IMAXDOS back to the background level LBASE. This point is

labelled A. The drift time is then taken to be a fraction K (currently 1/3) of the distance from point A to IMAXDOS.

The determination of the charge integrals, Q, of the two pulses must be carefully optimised because the charge collected at each wire end is not exactly proportional to the resistance between the struck point and the preamplifier. The pulses that travel from the struck point are initially identical and the connection is a dispersive transmission line rather than a simple resistance.

The signal in the first eight bins of each pulse are summed unless the pulse on either wire end is less than eight bins in length. In this case the sum is taken over the length of the shorter pulse. The summation is then corrected to begin at the drift time calculated above rather than at the edge of the first bin of the hit. The background integral is then subtracted using LBASE as calculated above. A detailed study of this algorithm may be found in [54].

The end result of this analysis is the MRTE (theta chambers) and MRPE (phi chambers) banks which contains the Qt hit information which is the starting point for the forward muon reconstruction.

Figure 4.10: The leading edge algorithm for finding the drift time from the raw pulse data. From [50].

The Forward Muon Reconstruction Code

With the determination of the Qt values, the online data acquisition ceases and all further analysis is carried out offline. This analysis is carried out in the framework of the main H1 reconstruction program, H1REC [35]. The H1 software is written in a modular fashion (as described in [55]) so that the code for each subdetector may be run independently. The module that performs the forward muon reconstruction is called MTREC. A complete technical description of this code may be found in [52].

Qt to Space Point Conversion

1) Drift Co-ordinate

The drift time delivered by the Qt algorithm is relative to the global event T_{zero} as determined by the trigger. It is necessary to correct for various delays in the system before converting to a drift distance by multiplying by the drift velocity. Hence, the expression used is

$$x_{drift} = v_{drift}(t_{drift} - t_{zero} - t_{jitter} - t_{tof})$$

where x_{drift} is the drift distance, v_{drift} is the drift velocity, t_{drift} is the drift time as given by the Qt analysis. The corrections are

1) t_{zero} , a global offset determined by the minimum drift time of a reference cell.

2) t_{jitter} , a wire by wire offset relative to the global t_{zero} , measured using test pulses.

3) t_{tof} , a correction based on the time of flight, the time taken for a photon to travel from the front plane of the detector to the plane of the hit.

For Monte Carlo, all three corrections are set to zero. The determination of these constants and the drift velocity for data will be discussed in a later section. Several assumptions are made in order to be able to use the above formula:

1) That the drift time to drift distance relationship is linear, or equivalently that the drift velocity is a constant across the cell. Studies [51] have shown that this approximation is not

valid unless the operating voltage of the chambers is chosen carefully.

2) That the electron that arrives first at the wire corresponds to the central plane of the cell. This may not the case for angled tracks, where the electron closest to the wire does not come from the central plane. This is further complicated by the change over from a relatively uniform drift field to a radial field near the wire. Ideally, what is needed is an *Isochrone Map* of the cell. An Isochrone is a line of constant drift time to the wire. This analysis is in progress. However, for the current level of understanding of the chambers, the above determination of the drift distance is sufficient.

3) That all cells have similar drift characteristics. This is expected to be the case as the cells differ in length, not cross section. Minor differences such as propagation times down the wire are included in the t_{jitter} correction.

The drift distance obtained by the above procedure corresponds to a distance from the wire of the struck cell, but no information is given on the sign of this drift. Therefore, the drift distance is added to and subtracted from the co-ordinate of the wire to give two ambiguous solutions. The error on each point is not calculable from the data directly and so is given to the program as a single value worked out by offline analysis, as described later. The design value for the drift co-ordinate resolution is 250 μm.

2) Charge Division Co-ordinate

The charge division co-ordinate is worked out by considering the resistance to ground seen by the pulses heading towards each wire end. Consider a hit as shown in figure 4.11, a distance x along the wire from the nearest preamp. The resistance seen by the pulse from cell 1 is

$$R_1 = R_{preamp} + R_x$$

where R_{preamp} is the input resistance of the preamplifier (in fact, the mean of the two resistances as this is all that can be measured) and R_x is the resistance between the preamplifier and the hit. The resistance seen by the pulse from cell 2 is then

$$R_{tot} - R_l = R_{preamp} + R_{wire1} + R_{link} + R_{wire2} - R_x$$

where R_{tot} is the total resistance of the pair given by

$$R_{tot} = R_{wire1} + R_{link} + R_{wire2} + 2R_{preamp}$$

R_{wire1} and R_{wire2} are the resistances of the two wires and R_{link} is the resistance of the link resistor. The fraction of the total resistance between the hit and the resistive centre of the system is given by the charge division ratio

$$Q_R = \frac{Q_1 - Q_2}{Q_1 + Q_2}$$

where Q_1 and Q_2 are the charges at the two wire ends. However, it is possible that the two preamplifiers have different gains, so this expression must be corrected by including the gain ratio, G, giving

$$Q_R = \frac{1 - G\frac{Q_1}{Q_2}}{1 + G\frac{Q_1}{Q_2}}$$

The resistance between the hit and the resistive centre is given by

$$\frac{R_{tot}}{2} - R_l - R_{preamp}$$

and hence R_l is given by

$$R_l = \frac{R_{tot}}{2} - Q_R\left(\frac{R_{tot}}{2}\right)\left(\frac{L_{effective}}{L}\right) - R_{preamp}$$

where ($L_{effective}$ / L) is a measurable correction factor included for compatibility with the central tracker analysis only. It is equal to unity for the forward muon system at the present level of

understanding.

Having calculated R_l in this fashion, x, the distance of the hit from the preamplifier end of the struck cell, is given by

$$x = R_l \left(\frac{L_{wire1}}{R_{wire1}} \right)$$

where L_{wire1} is the length of wire in cell 1. This is then added to the co-ordinate of the preamplifier end of the cell to give the charge division co-ordinate.

As for the drift co-ordinate, the error on the charge division co-ordinate is not calculable directly from the data. The error varies with the length of the wire and is thus given as a fraction of the total wire length (length of wire in cell 1 plus length of wire in cell 2 plus the length of wire equivalent to the link resistor). Single-ended hits (with one charge value of zero) are placed at the preamplifier end of the struck cell with an error of 5% of the wire length. The design resolution is 1% of total wire length.

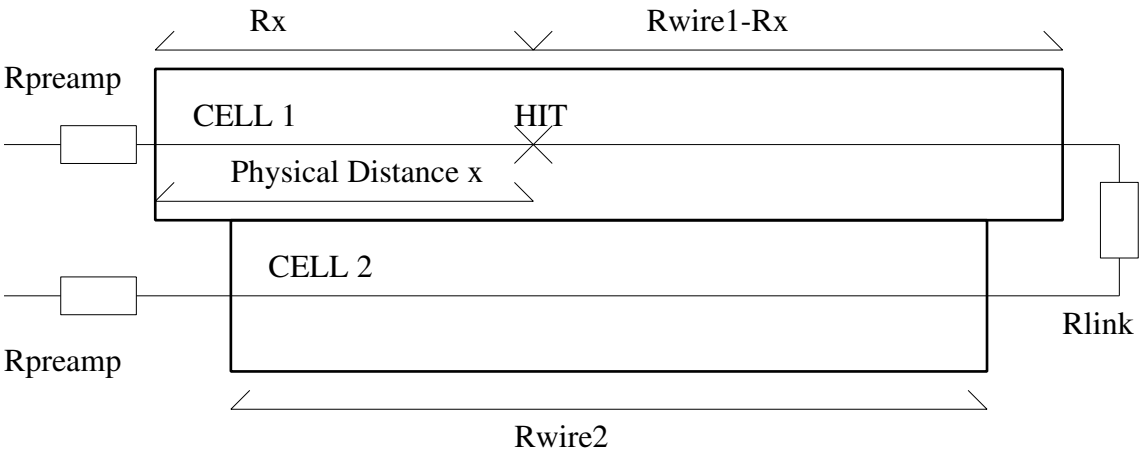

Figure 4.11 : Resistance division in a hit pair. The hit is a distance x along the wire from the nearest preamplifier.

The Pairing Algorithm

The pair finding algorithm attempts to associate hits on each side of a double layer. Only hits within one octant of the double layer are considered. Although there is some overlap between octants, this does not affect the pair finding significantly as a pair would be found in both octants and the best fit of these used in segment finding. As the overlap between octants is small, only a small fraction of events would have better information by including these extra pairs.

For each hit in the octant and layer, a search is performed for hits in the other side of the layer which lie within a distance δx (nominally 15.0 cm) in the charge-division co-ordinate and δy_l (nominally 5.0 cm) in the drift co-ordinate. Single-ended hits may be discarded or accepted by the pairing routine based upon a user-supplied parameter. The co-ordinate system used is local to the octant with y radially outwards, z along the H1 z axis and x defined so as to make a right-handed co-ordinate system. The origin of the co-ordinate system is the nominal beam position in x,y and the centre of the octant frame in z. This co-ordinate system is the natural one for the task, as it does not introduce any mixing between drift and charge division co-ordinates.

The cut in drift distance ensures that the segments found will be flat, that is, below a certain theta angle given by $\tan^{-1}(\delta y_l/\delta z)$ at the centre of the cell, where δz =3.42 cm, the separation between wire planes. Thus track segments with theta angle greater than ≈56° will not be recognised at the pairing stage. This is to reduce combinatoric problems as in principle all possible combinations of drift sign resolution are valid so long as the track is steep enough. Tracks from the H1 vertex should emerge from the iron with θ<20°, but segments after the toroid may be steeper than this due to bending in the magnetic field and multiple Coulomb scattering in the iron toroid.

Any pair satisfying the above cuts will be considered, but it is possible that more than one resolution of the drift sign ambiguity satisfies the cut for any given pair. An example of this is shown in figure 4.12 where the hit is close to the wire in the left hand side of the layer. In order to reduce this effect, a second pass is performed to reject some of the steeper candidates. If the difference in y is greater than a second cut, δy_t,(nominally 1.5 cm) and there is another

candidate with a smaller y difference, only the candidate with the smaller δy is taken. In the case of figure 4.12, both candidates would be accepted as both are within the tighter y cut.

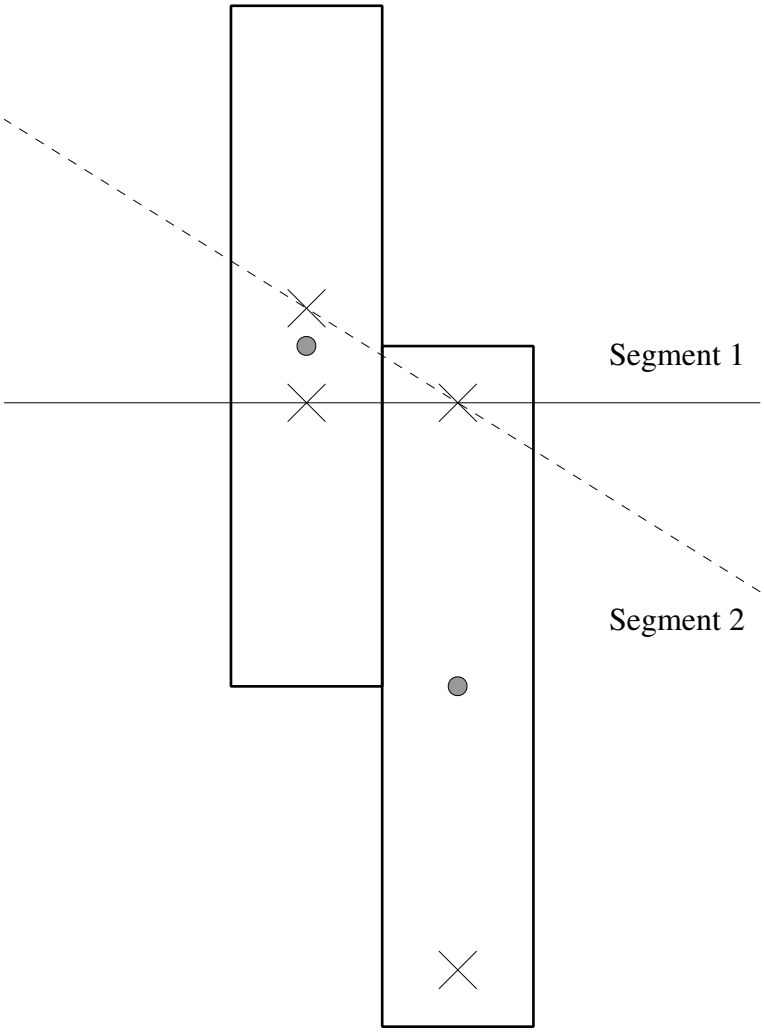

Figure 4.12: Multiple pairing possibilities. The drift resolution in the right hand cell is obvious, but it is not clear which solution to choose for the left hand cell as segment 1 and segment 2 are both valid possibilities.

The above scheme is also suitable for finding beam halo tracks, that is, real muon tracks that come in time with the proton beam and form a halo around the beam. These tracks, which are almost horizontal ($\theta \approx 0°$), are very useful for alignment and calibration studies. However, the scheme is not suitable for cosmic muon tracks, which are usually steep. In order to be able to reconstruct cosmics, the y cuts must be opened up to $\delta y_t = \delta y_l = 10.0$ cm to allow steep segments to

be found.

Pair finding in the phi chambers is complicated somewhat by the sliders, which mean that the phi layers effectively have three 'sides'. A search for pairs is therefore made in sides 1 and 2, 1 and 3 and finally 2 and 3.

The Segment Finding Algorithm

The segment finding algorithm relies on finding a segment between two theta layers and then associates any information from the intervening phi layer afterwards. The reason for this is historical: initially, only the theta layers were installed. All 1992 H1 data were taken with the theta layers only. The phi layers were installed in the 1992-1993 shutdown and are now fully operational. In principle, a more complex pattern recognition algorithm could be used to pick out tracks by requiring a certain number of hits along a straight line, regardless of whether they lie in theta or phi chambers. However, a good θ measurement is necessary for accurate momentum determination so any segments found without at least three theta hits are not useful. The straight-forward algorithm used provides this minimum of three theta hits.

The search proceeds by looping over all theta pairs and trying to find a hit, paired or unpaired, in the other theta layer (i.e. for a pair in theta one, search in theta two) in the same or one of the adjacent octants.

For each hit combination, the ϕ co-ordinate and error in phi of each pair is worked out. From this, the difference in ϕ co-ordinates of the two pairs, $\delta\phi$, and the error on that difference, $\Delta\delta\phi$, are worked out. The error on the ϕ difference is required to be less than a a cut E_{seh}, nominally 5.0 degrees, which ensures that the segment is reasonably well defined. This is mainly to exclude segments made solely with single-ended hits, which have a large error on the charge division co-ordinate. A test is also made to ensure that the segment is roughly radial by insisting that the ratio $\delta\phi/\Delta\delta\phi$ be less than a cut, nominally 10.0. This ensures that the pairs are close to each other in ϕ within errors.

For all segments passing these criteria, a straight line fit is made in *x-z* (charge division) and *y-z* (drift). The quality of the fit is assessed by the chi-squared method [59]. Given a set of

values, y_i, measured at a set of points, x_i and a functional form of $y=f(x)$, χ^2 is given by

$$\chi^2 = \sum_i \sum_j \left(y_i - f(x_i)\right) V^{-1}_{ij} \left(y_j - f(x_j)\right)$$

where V^{-1}_{ij} are the elements of the inverse of the covariance matrix **V**. In the simple case where the measurements are independent, **V** and $\mathbf{V}^{-1}$ are diagonal and the expression reduces to

$$\chi^2 = \sum_i \frac{\left(y_i - f(x_i)\right)^2}{\sigma_i^2}$$

where σ_i are the estimated errors on the measurements y_i.

The χ^2 values from the the two fits are added together to give the total value of χ^2 for the segment. The hits are all transformed to the local co-ordinates of the original pair before fitting but full covariance information is preserved. If the χ^2 is less than a cut value χ^2_{max} (nominally 100.0) multiplied by the number of hits on the segment, the segment is accepted.

A loop is then made to check for using hits twice with different drift ambiguity. All segments with χ^2 less than a cut (nominally 10.0) are kept. Segments which share the same hits but have χ^2 greater than this cut are compared. If the χ^2 of the worse fitted segment is at least a factor (nominally 4.0) greater than the better segment, it is rejected.

Once segments have been found using the theta information, the segment is extrapolated to the plane of the phi layer in between the two theta chambers. The same procedure as used above is now used to associate phi hits to the segment, with $\delta\phi$ being the difference between the extrapolated segment ϕ-coordinate and the ϕ-coordinate of the phi chamber pair. If this satisfies cuts, the x-z and y-z fits are re-done including the phi hits, and a new χ^2 formed. If this χ^2 is less than χ^2_{max} multiplied by the new number of hits, the segment is accepted. If more than one phi pair satisfies the association criteria, only the combination with the lowest χ^2 is accepted. If no phi pair was associated or the combinations had too high a χ^2, the theta segment is output as found in the earlier stage.

Track Finding And Momentum Determination

To find tracks, all segments are first extended in a straight line to the centre of the toroid. A search is then made for segments on the other side of the toroid whose intersection with this plane lie within a difference in radius δr (nominally 20.0 cm) and a difference in the phi co-ordinate of $\delta\phi$ (nominally 30.0°). The code checks to see whether there are more segments before or after the toroid in order to decide whether to extrapolate from before the toroid to after the toroid or vice versa. If there are more segments before the toroid only the segments after the toroid will be extrapolated. This is normally the case for real data where particles have been sprayed up into the detector from the beamline magnets and sail-through and punch-through from the instrumented iron is significant. This is the case that will be discussed, although both cases are implemented in the code.

The extrapolation proceeds by tracking the segment back to the face of the toroid, then extrapolating through the toroid in small steps (normally 15 steps are used). This extrapolation is done for a range of candidate momenta from 2.25 GeV to 1000.0 GeV and for both muon charges. As there is no sensitive volume in the toroid for tracking particles, it is necessary to evaluate where a muon of given charge and momentum will emerge from the toroid on average and calculate the expected deviation from the average position due to multiple scattering. This is then compared with the segment on the other side of the toroid. The deviation in angle, $\delta\theta$, caused by a magnetic field of field strength B Tesla is

$$\delta\theta = \frac{0.003\ B\ \delta l}{p}$$

where p is the muon momentum in GeV/c and δl is the distance travelled in the field in cm. In extrapolating through the toroid the radial and z-components of the magnetic field are taken to be zero and it is assumed that the field is zero outside the iron.

The muon momentum is recalculated for each step in the extrapolation to take account of the energy lost in traversing the iron [56]. The energy loss for a muon in various materials as a function of momentum is shown in figure 4.13.

Figure 4.13: The average energy loss of a muon per g/cm^2 of hydrogen, iron and uranium as a function of muon energy. Contributions of several processes to dE/dx in iron are also shown: (p) direct e^+e^- pair production, (b) bremsstrahlung, (n) photonuclear interactions and (i) ionization. From [57].

In addition to the energy loss, the accumulated error due to Coulomb multiple scattering is calculated. This provides an estimate of the expected scatter on the extrapolated segment and is used in conjunction with the errors on the segments to calculate χ^2 for the track candidate. A Gaussian approximation to the Moliere theory [58] of multiple scattering is used. The width of this Gaussian is θ_0, given by [57]

$$\theta_0 = \frac{0.0136 \text{ GeV/c}}{p\beta} Z_{inc}\sqrt{\frac{L}{L_R}}\left[1 + 0.038 \ln\left(\frac{L}{L_R}\right)\right]$$

where p is the particle momentum in GeV/c, β is the velocity in units of c, Z_{inc} is the charge of the incident particle in units of e, L is the distance traversed and L_R is the radiation length of the scattering medium. In this approximation θ_0 is the r.m.s. value of θ_{plane}, as shown in figure 4.14.

Figure 4.14: Multiple scattering in a plane. From [57].

The random values s, ψ, y and θ as shown in this figure are correlated and these correlations are retained throughout the extrapolation to produce a full covariance matrix for comparing the segment before the toroid with the extrapolated segment.

The above approximation is good to 11% for $10^{-3} < L/L_R < 100$ except for light elements and when the velocity is very small. Typically, 15 steps are used in the extrapolation, giving a length 8 cm for a track normally incident on the toroid. The radiation length of iron is 1.76 cm, so the ratio $L/L_R = 4.5$, within the validity of the approximation. The main source of deviation from this approximation is the occurrence of single large angle scatters, giving a much broader tail to the distribution than is the case for a Gaussian. These tails are a few percent in the regions where the Gaussian has become negligible.

Once the extrapolations have been done, all segments within the δr, $\delta\phi$ cut are compared with the extrapolated segments and a χ^2 is formed for each. This results in a χ^2 versus momentum plot. A quadratic fit is then made to the point corresponding to the minimum value of χ^2 found in the scan and the points in the scan either side of this minimum. The true minimum value of χ^2 is then calculated from this fit and the track candidate assigned a momentum corresponding to this value of χ^2. The track candidate is accepted if it has a χ^2 lower than a cut, nominally 75.0. If more than one segment is associated to the original segment, only the candidate with the lowest χ^2 is accepted.

Once all track candidates have been found, a search is performed to reject multiple tracks formed from the same hits. If more than one track uses an individual hit (including tracks which use different drift signs of the same hit), only the track with the lowest χ^2 is accepted.

The forward muon subdetector reconstruction is now complete and the information is written out in the MTKR BOS-bank.

Event Display Routines

Besides having all relevant information for the track in banks, it is essential to display this information visually. Therefore, subroutines were written for forward muon subdetector displays to fit within the framework of the main H1 event display program, H1ED [48]. This uses the LOOK graphical display system [41] as a histogramming package and interface to the graphics primitives, in this GKS graphics [47].

Options exist to view the chambers radially or in side views, and the granularity of the displays may be changed to show all cell boundaries or just octant outlines. It is possible to display single octants, whole layers or the whole detector. It is also possible to superimpose on the display the information on the Monte Carlo true hits. The structure of the LOOK program makes it easy to define more complex displays from combinations of simple displays.

Tzero And Drift Velocity Determination

The procedure used to determine the calibration constants (drift velocity and t_{zero}) of the forward muon chambers is detailed in [51]. The basic principle is that uniform illumination of a cell at normal incidence, uniform efficiency and constant drift velocity produces a time distribution of hits whose width in time corresponds to the full drift distance of 6cm and whose rising edge is at the appropriate t_{zero} for that cell. The distribution should have a flat plateau.

Deviations from this ideal behaviour occur if the drift velocity varies near the wire (or at the cell edge) or the tracks deviate from normal incidence. These effects, combined with a finite drift time resolution, smear the edges of the distribution and therefore make t_{zero} extraction more difficult. Any deviation from uniform efficiency, uniform illumination or constant drift velocity across the body of the cell changes the plateau of the distribution so it is no longer flat. If uniform illumination and efficiency are assumed, the drift time distribution may be used to extract the drift time to drift distance relationship. For this case, the time distribution may be divided into *N* equal time bins and the relationship

$$x_p = \frac{\Delta x}{N} \sum_{i=0}^{p} n_i$$

then holds, where x_p is the distance corresponding to the p^{th} time bin, Δx is the total drift distance and n_i is the number of hits in the i^{th} time bin. This procedure was used with a test setup to determine what value of the electric field should be used to provide as uniform a drift velocity as possible. The value chosen for the Autumn 1992 run was 0.45 kV cm^{-1}.

The other method used for calibration uses checksums based upon the fact that segments are straight lines and thus the drift times of the hits on a segment are therefore related. This may be used to extract an independent value of t_{zero} and also to provide a measurement of the spatial resolution of the chambers.

The values obtained for the Autumn 1992 run were (from [50]) t_{zero} = 216 ± 5 ns and v_{drift} = 4.93 ± 0.04 cm μs^{-1}. The r.m.s. drift distance resolution obtained was 310 ± 5 μm, compared with the design value of 250 μm.

Chamber Alignment

Finding the alignment of the forward muon system is not straightforward, as there is insufficient space around the chambers to allow a detailed survey. This means that the bulk of the alignment must be done using tracks in the detector. However, in 1992, only the theta chambers were installed and as this only gives a maximum of four hits on a segment, there is very little redundant information to work with. Alignment is done using beam halo tracks taken during dedicated runs with no field in the toroid to allow relative alignment of chambers before and after the toroid. The alignment procedures used are described in detail in [50].